In vitro structure-toxicity relationship of chalcones in human hepatic stellate cells

Title: *In vitro* structure-toxicity relationship of chalcones in human hepatic stellate cells

Author: Katharina Zenger Subhajit Dutta Horst Wolff Marc G. Genton Birgit Kraus

PII: S0300-483X(15)30018-4
DOI: http://dx.doi.org/doi:10.1016/j.tox.2015.07.012
Reference: TOX 51572

To appear in: *Toxicology*

Received date: 16-5-2015
Revised date: 14-7-2015
Accepted date: 15-7-2015

Please cite this article as: Zenger, Katharina, Dutta, Subhajit, Wolff, Horst, Genton, Marc G., Kraus, Birgit, In vitro structure-toxicity relationship of chalcones in human hepatic stellate cells.Toxicology http://dx.doi.org/10.1016/j.tox.2015.07.012

In vitro structure-toxicity relationship of chalcones in human hepatic stellate cells

Katharina Zenger [a], Subhajit Dutta [b], Horst Wolff [c], Marc G. Genton [b], Birgit Kraus [a,*]

[a] Pharmaceutical Biology, Institute of Pharmacy, University of Regensburg, Regensburg, Germany

[b] CEMSE Division, King Abdullah University of Science and Technology, Saudi Arabia

[c] Carl Zeiss Microscopy GmbH, Göttingen, Germany

*Corresponding author: Phone: ++49 (0)941 9434494

E-mail address: birgit1.kraus@chemie.uni-regensburg.de

Abstract

Xanthohumol (XN), the major prenylated chalcone from hops (*Humulus lupulus* L.), has received much attention within the last years, due to its multiple pharmacological activities including anti-proliferative, anti-inflammatory, antioxidant, pro-apoptotic, anti-bacterial and anti-adhesive effects. However, there exists a huge number of metabolites and structurally-related chalcones, which can be expected, or are already known, to exhibit various effects on cells. We have therefore analyzed the effects of XN and 18 other chalcones in a panel, consisting of multiple cell-based assays. Readouts of these assays addressed distinct aspects of cell-toxicity, like proliferation, mitochondrial health, cell cycle and other cellular features. Besides known active structural elements of chalcones, like the Michael system, we have identified several moieties that seem to have an impact on specific effects and toxicity in human liver cells *in vitro*. Based on these observations, we present a structure-toxicity model, which will be crucial to understand the molecular mechanisms of wanted effects and unwanted side-effects of chalcones.

Keywords

chalcones; structure activity relationship; xanthohumol; hepatic stellate cell

Abbreviations

3OH-Heli, 3-hydroxy-helichrysetin; 3OH-XNH, 3-hydroxy-xanthohumol H; 3OMe-XNH, 3-methoxy-xanthohumol H; 4Ac-XN, 4-*O*-acetyl-xanthohumol; 4Me-XN, 4-*O*-methyl-xanthohumol; 4´Me-XN, 4´-*O*-methyl-xanthohumol; C, cardamonin; dhFKC, dihydro-flavokawain C; dhHeli, dihydro-helichrysetin; dhXNC, 1'',2''-dihydro-xanthohumol C; FKA, flavokawain A; FKB, flavokawain B; FKC, flavokawain C; HCA, High-content analysis; Heli, helichrysetin; HSC, hepatic stellate cells; P, pinostrobin chalcone; PBS, phosphate buffered saline; PFA, paraformaldehyde; thXNC, dihydro-1'',2''-dihydro-xanthohumol C; XN, xanthohumol; XNC, xanthohumol C; XNH, xanthohumol H;

1. Introduction

Chalcones (1,3-diaryl-2-propen-1-ones) are open-chain flavonoids, more precisely they constitute flavanone precursors with open C ring, which arise from a mixed biosynthesis including both the shikimate and the acetate malonate pathway. They represent an exceptional class of structural templates that exhibits a wealth of biological functions, which include anti-inflammatory, antioxidant, anti-microbial and anti-tumor activity. Excellent and comprehensive overviews over pharmacological activities of chalcones are given elsewhere (Batovska and Todorova, 2010; Dimmock et al., 1999; Orlikova et al., 2011; Sahu et al., 2012; Xie et al., 2015).

As minor constituents, chalcones are ingested via dietary sources (e.g. tomatoes (Yamamoto et al., 2004), citruses (Iwase et al., 2001), apples (Gaucher et al., 2013)) or herbal drugs (e.g. willow bark (Freischmidt et al., 2012), liquorice (Furusawa et al., 2009), and kava root (He et al., 1997)). Due to its occurrence in hops (*Humulus lupulus* L.) and beer (Magalhães et al., 2009), and its many pharmacological properties (Gerhauser et al., 2002; Legette et al., 2014; Liu et al., 2015), xanthohumol (XN) is one of the best known and investigated prenylated

chalcones of the past decade. It received much attention in the recent years, as it was identified as a broad-spectrum cancer chemopreventive agent. Moreover, XN was shown to reduce hepatic inflammation and fibrogenesis in a mouse model. Furthermore, it had an influence on hepatic stellate cells (HSC), which are central mediators of fibrosis and might serve as a target for the treatment of liver fibrosis. Cell treatment with XN inhibited activation of HSC and in activated HSC apoptosis was induced (Dorn et al., 2010).

In contrast to many other chalcones, the metabolism of XN was extensively studied, and both *in vitro* and *in vivo* studies have been conducted (Hanske et al., 2010; Henderson et al., 2000; Yilmazer et al., 2001a, 2001b). These studies have revealed, that on the one hand XN is a potent inhibitor of P450 enzymes (Henderson et al., 2000), but on the other hand it is also heavily metabolized by liver cells (Hanske et al., 2010; Nikolic et al., 2005) and microorganisms (Kim and Lee, 2006; Nookandeh et al., 2004) into several other, prenylated and non-prenylated chalcones.

It is largely unknown, which structural elements within XN or related chalcones, are causing which effects. Michael type additions seemed to be the most promising candidates to explain specific effects of chalcones in eukaryotic cells. It was shown that they contribute to accumulation of XN in cells and can alter cellular processes (Harikumar et al., 2009; Pang et al., 2007; Wolff et al., 2011). However, chalcones also exhibit a variety of other interesting motifs which are expected to influence toxicity on cells and also likely promote other cellular effects.

Very recently, quantitative structure-activity data have been generated, regarding anti-oxidant (Das et al., 2014) and anti-cancer (Jung et al., 2015) effects of flavonoids and analogues. While this is valuable data, we followed a broader approach, addressing multiple cellular properties related to cell-toxicity, caused by several structurally related chalcones. This approach has the potential to provide deep insight into cellular impacts that occur, when chalcones are presented to HSC. It also allows an estimation which modifications at the chalcone-scaffold will be more or less toxic to cells.

We therefore chose a set of natural and synthetic chalcones with different aryl substituents such as hydroxy- (OH), methoxy- (OMe), and prenyl-groups and exposed a panel of four cell-based assays, resulting in seven cellular features, to XN and 18 other chalcones. All cellular assays were carried out with a human hepatic stellate cell line (Hellerbrand, 2013; Schnabl et al., 2002) and were designed to be suitable for high-content screening procedures. High-content analysis (HCA) is a combination of cell-based assays, fluorescence imaging, automation and advanced image analysis. In contrast to assays with single readouts, HCA is able to measure multiple biological pathways and features simultaneously, or to reveal off-target effects of compounds (Bickle, 2010; Zock, 2009). Due to its high degree of automation, it supports generation of sufficiently large data to make statistically relevant conclusions.

Finally, we present a model that sets functional groups of chalcones in relation to several distinct toxicity-related cellular phenotypes.

2. Material and methods

2.1. Cell and cell culture

The immortalized activated human hepatic stellate cell line (HSC) (Schnabl et al., 2002) was kindly provided by the group of Claus Hellerbrand (University Hospital of Regensburg, Department of Internal Medicine I). HSC were kept under standard cell culture conditions (37°C, 5% CO_2, humified atmosphere) using Dulbecco's Modified Eagle Medium (Invitrogen, Karlsruhe, Germany) with 10% heat-inactivated fetal calf serum (FCS) and 2 mM glutamine (Biochrom, Berlin, Germany).

2.2. Compounds

XN was purchased from Nookandeh Institute (Homburg, Germany), pinostrobin chalcone from Phytolab (Vestenbergsgreuth, Germany). Synthesis of all remaining chalcones was

performed at our institute and described previously (Vogel and Heilmann, 2008; Vogel et al., 2010, 2008). Chemical structures of tested chalcones are shown in **Figure 1.**

Xanthohumol (**1**, XN) is the major chalcone in hops (*Humulus lupulus*) (Liu et al., 2015). 4-*O*-acetyl-xanthohumol (**2**, 4Ac-XN), 4-*O*-methyl-xanthohumol (**3**, 4Me-XN), xanthohumol H (**5**, XNH), xanthohumol C (**8**, XNC), and 1'',2''-dihydro-xanthohumol C (**9**, dhXNC) were found as metabolites of XN in rat feces (Nookandeh et al., 2004) and may also occur in humans after administration of XN *in vivo*. 3-Hydroxy-xanthohumol H (**6**, 3OH-XNH) and 3-methoxy-xanthohumol H (**7**, 3OMe-XNH) are synthetic derivatives of the metabolite XNH. 4´-*O*-methyl-xanthohumol (**4**, 4´Me-XN) does not occur naturally and is a prenyl structure analogue of flavokawain C (**14**, FKC). Xanthohumol C (**8**, XNC), 1'',2''-dihydro-xanthohumol C (**9**, dhXNC), and FKC (**14**) were found as minor constituents in *Humulus lupulus* (Chadwick et al., 2004; Stevens et al., 2000). FKC (**14**), as well as flavokawain A (**12**, FKA) and flavokawain B (**13**, FKB), occur naturally in *Piper methysticum* FORST. Cardamonin (**16**, C) can be found in *Alpinia rafflesiana* WALL. EX BAKER (Mohamad et al., 2004). Pinostrobin chalcone (**15**, P) was identified in *Alpinia mutica* ROXB. rhizome (Malek et al., 2011). Helichrysetin (**10**, Heli) is a natural chalcone derived from *Helichrysum odoratissimum* L. (Van Puyvelde et al., 1989), and 3-hydroxy-helichrysetin (**11**, 3OH-Heli) is a synthetic derivative with a catecholic substitution of the B ring. In addition, three synthetic dihydrochalcones, dihydro-flavokawain C (**17**, dhFKC), dihydro-helichrysetin (**18**, dhHeli), and dihydro-1'',2''-dihydro-xanthohumol C (**19**, thXANC), which have an α,β-unsaturated ketone structure element, were also included.

2.3. MTT assay

For determination of cell viability, MTT (3-(4,5-dimethylthiazol-2-yl)-2,5-diphenyl tetrazolium bromide) assay was adapted to previously described procedures (Mosmann, 1983). In brief, $5x10^3$ cells/well were seeded in a 96-well plate and cultured for 24 h under standard cell culture conditions. Then cells were treated for 24 h with the different chalcones at concentrations of 1, 10, 25 and 50 µM and kept under the same conditions as before. After treatment and removal of the incubation medium, cells were incubated with 100 µL MTT solution (0.4 mg/mL) per well. After 3 h at 37°C, supernatants were removed and 100 µL lysis buffer (10% SDS, pH 4.1) was added to each well. Plates were stored at room temperature in a dark place and the next day absorbance of the formazan solution was measured with a plate reader at 560 nm. Absorption of test wells was normalized to values from untreated wells on the same plate.

2.4. High-content image acquisition and analysis (HCA)

In this study, fluorescence microscopy was applied to investigate the influence of the test chalcones on cell organelles of HSC. Cells were transferred into 96-well plates at $5x10^3$/well, and treated for 24 h with different chalcones at concentrations of 1, 10, 25 and 50 µM. Cells were incubated with 50 µL/well of a 1:2000 dilution of MitoTracker Red CMXRos® (Life Technologies, 1 mM stock solution) for 25 min at 37 °C. This mitochondrion-selective, rosamine-based probe passively diffuses across the plasma membrane and accumulates in active mitochondria. It is not washed out after fixation and permeabilization steps. Subsequently, 25 µL/well of Hoechst33342 staining solution (Sigma, bisbenzimide H33342 trihydrochloride, 20 mM, 1:1200) was added to the wells for 5 min. Hoechst33342 counterstain is used to determine nucleus area and shape, and the staining intensity can be used for determination of cellular DNA content. Next, the staining solution was aspirated and cells were washed with 100 µL/well of pre-warmed phosphate buffered saline (PBS). Afterward, cells were fixed with 100 µL/well of 3% paraformaldehyde (PFA) for 30 min at room temperature. Cells were washed again with PBS and then treated for 2 min with 50

µL/well of permeabilization buffer (0.1% Triton® X-100 in PBS). After a further washing step, the cellular actin filaments were stained with an Alexa Fluor® 488 labeled phalloidin (Life Technologies). Bicyclic phallotoxins from *Amanita phalloides* label F-actin at nanomolar concentrations in a stoichiometric ratio, which makes them also suitable to quantify the amount of F-actin in cells. The methanolic stock solution (200 units/mL) was diluted 1:50 with staining medium and 35 µL were added to each well for 20 min at room temperature. Solution was aspired and cells were washed thoroughly with PBS. At the end, 100 µL of PBS were added to each well for image acquisition.

Subsequently, images were acquired with a fully motorized ZEISS Cell Observer(R) (Carl Zeiss, Germany) system and a 10x Plan-NeoFluar objective. Filter set No. 49 (Ex: 360/40; FT 400; Em: 460/50) was used to acquire images of blue fluorescent Hoechst33342-stained cell nuclei. Filter set No. 38 (Ex: 475/40; FT 500; Em: 530/50) was employed to acquire images of green fluorescent Alexa Fluor 488-labeled actin, and filter set No. 43 (Ex: 550/25; FT 570; Em: 605/70) served to take images of red fluorescent MitoTracker-labeled mitochondria.

Measurement features were extracted from individual cells of at least 4 randomly selected fields of view per well. Cells in untreated control wells of the same plate were used as controls and treatment-caused alterations were set in relation to this.

Quantitative high-content image analysis was carried out using the “Physiology Analyst” function of the ASSAYbuilder module (powered by Cellomics) of software AxioVision 4.7.1 (Carl Zeiss, Germany). Details can be found in the manufacturer´s protocols and the user´s guide. Briefly, cell nuclei (stained with Hoechst33342) were automatically detected by the software. A nuclear mask was generated and used to detect fluorescence in the nucleus. A ring mask with a fixed width around the nucleus was used to quantify fluorescence in the cytoplasm. Nuclear and cytoplasmic masks were used to automatically extract a variety of cellular features in all fluorescence channels of the images.

2.4.1. Cytochrome c assay

For the determination of cytochrome c release from mitochondria of apoptotic cells, the Cellomics® Cytochrome C Detection kit (Thermo Fisher Scientific) was applied followed by fluorescence microscopic high-content analysis. The assay was conducted according to the manufacturer's protocol with slight modifications. After treatment, cells were fixed with 4% PFA (100 µL/well) for 15 min at room temperature. Fixation solution was aspirated and cells were washed twice with Wash Buffer. Following, cells were incubated with permeabilization Buffer (100 µL/well) for 15 min at room temperature. Again, the buffer was aspirated and cells were washed twice with Wash Buffer. Subsequently, cells were treated with Blocking Buffer (+ 2% FCS, 100 µL/well) for 15 min at room temperature and then incubated with Primary Antibody Solution for 1 h at room temperature. After removal of the antibody solution, the plate was washed twice with Wash Buffer II and Wash Buffer respectively. Staining with Secondary Antibody Solution was performed for 45 min at room temperature. Images were acquired with a fully motorized ZEISS Cell Observer(R) system and a 10x Plan-NeoFluar objective. Filter set No. 49 (Ex: 360/40; FT 400; Em: 460/50) was used to acquire images of blue fluorescent Hoechst33342-stained cell nuclei and filter set No. 43 (Ex: 550/25; FT 570; Em: 605/70) was used to take images of red fluorescently labeled cytochrome c. In normal cells, cytochrome c is located in the mitochondria, which can be detected as cytoplasmic spots. Upon induction of apoptosis, cytochrome c is released from the mitochondria and can diffuse into the nucleus. Thus, a reallocation of stained cytochrome c is detectable. Image analysis was automatically done by the ASSAYbuilder Physiology Analyst software as described above. A circular mask was put over the nucleus area and a ring mask over the cytoplasmic area of a cell. The ring mask measures the fluorescence in the cytoplasm of cells where unreleased cytochrome c within the mitochondria can be found. The circular mask determines the fluorescence in the nucleus area of cells where cytochrome c diffuses when it is released from the mitochondria. To determine the reallocation and therefore the extent of released cytochrome c, the mean average fluorescence intensity between difference between nucleus and cytoplasm was calculated.

Staurosporine, which is known to trigger cytochrome c release from apoptotic mitochondria, was used as a positive control. Control cells were treated for 4 h with 1 µM staurosporine. All values of chalcones were normalized to that of staurosporine, which was set as 100% cytochrome c release.

2.4.2. DNA content/cell cycle state

DNA content was analyzed by measuring the intensity of Hoechst33342 nucleus staining by acquiring images at 10x magnification with a ZEISS Cell Observer$^{(R)}$ and filter set No. 49 (Ex: 360/40; FT 400; Em: 460/50). As the fluorescence intensity directly correlates with the DNA content (when the staining is in the linear range), conclusions concerning the actual cell cycle state can be drawn. Analysis of the cell cycle status was done using the "Cell Cycle Analyst" function of the ASSAYbuilder module. The ratio of cells with 2N and 4N DNA content was calculated and compared to untreated control cells with a 2N/4N ratio of 3.3. The 2N/4N ratio is a commonly used value in cell cycle analysis to describe influences on cell cycle phase distribution. An increase of the ratio indicates an arrest in G_1/G_0 whereas a G_2/M arrest is reflected by a decrease of this ratio (Gasparri et al., 2006).

2.5. General statistics and analysis of cell-based assays

If not mentioned otherwise for the data subjected to statistical analysis, experiments were conducted in (at least) triplicates and repeated independently not less than three times. The results of the assays are presented as the mean ± SD. For cell-based assays untreated control cells referred as 100% values. Statistical analysis was performed with GraphPad Prism 4. Gaussian distribution of values was tested prior to statistical analysis. Data were subjected to one-way ANOVA followed by Dunnett´s multi-comparison post-hoc test. P-values ≤ 0.05 were considered as statistically significant.

2.6. Computation of correlations between structure and toxicology using ANCOVA

ANCOVA (analysis of covariance) with no interaction was used for testing significances of treatment effects. ANCOVA extends the idea of blocking to continuous explanatory variables, as long as a simple linear mathematical relationship holds between the control variable and the outcome. Briefly, an R-script was used to calculate significances using multiple regression analysis with one categorical explanatory variable (functional group) and multiple quantitative control variables (treatment concentrations with distinct chalcones) to gain power. *P*-values of ≤ 0.05 were considered statistically significant.

3. Results

We chose a series of cell-based assays and cellular features to assess a broad range of potential cytotoxic effects of chalcones. To reveal an impact on cell viability of the entire cell population, we employed the well-known and established MTT assay. We complemented this information with automatic cell counts, based on microscopic images, to discover any effects that will result in lower proliferation but high cell metabolic activity or vice versa. We used these two assays to determine IC_{50} values of the chalcones of interest and to define the range of concentrations for subsequent assays.

Three further very sensitive parameters were employed to broaden our view on general cellular toxicity and perturbations. Nuclear DNA-staining allowed us to determine the size/area of the nucleus, as well as the DNA-content and thereby the cell cycle state of individual cells (Gasparri et al., 2006). In eukaryotic cells, actin fulfills very diverse and crucial functions (Field and Lénárt, 2011). We therefore stained the cells for F-actin to detect any abnormalities in the cell morphology or actin-associated functions, by using the total cellular amount of F-actin as a measure. Mitochondrial health was observed with a membrane-potential dependent mitochondrial dye. Thereby changes in mitochondrial mass can be visualized, which usually correlate with disturbed mitochondrial functions (Scatena, 2012). Finally, to understand better how and to which extent chalcones affect mitochondria, we

analyzed whether there was a cytochrome c release from mitochondria, enabling us to determine e.g. the state of apoptosis (Xiong et al., 2014).

For our studies, we have chosen a panel of chalcones, which are all closely structurally related (**Figure 1**). We evaluated toxicity and determined IC_{50} values by both, automatic cell counts (dose response experiments up to 50 µM) and MTT assay (dose response experiments up to 100 µM). Results are given in **Table 1**.

FKB (**13**) and 4´Me-XN (**4**) had the strongest influence on cell viability and cell proliferation with IC_{50} values of 39 and 30 µM respectively, while seven other chalcones had an IC_{50} between 50 and 100 µM, and for the remaining ten, the IC_{50} was higher than 100 µM.

Table 2 summarizes the influence of chalcones on seven assay readouts, including impact on viability, proliferation, nucleus area, actin-filament area, mitochondrial mass, cytochrome c release and cell cycle. The extent of influence in each case is indicated, differentiating between significant increase of readout at a compound concentration of 50 µM, significant increase at 25 µM or lower concentration, significant decrease at 50 µM, significant decrease at 25 µM or lower concentration, or no significant influence up to a compound concentration of 50 µM. Chalcones were grouped into eleven different clusters according to the influence patterns for all features.

Within one chalcone, presumably many structural motifs will contribute to the observed patterns. What is observed is likely a cumulative effect of several motifs, either adding up to a stronger total effect, or resulting in a reduced phenotype due to opposing activities of motifs within the same compound. **Figure 2** depicts this information in a graphical way. Individual compounds are grouped and up- and down-regulation of assay readouts is indicated. Detailed results of dose-responses of all compounds in the assays are given in **Supplementary Figure 1-19**.

In brief, we observed that XN (**1**) treatment leads to apoptosis in activated human hepatic stellate cells (HSC). Interestingly, a similar effect was also observed for the XN metabolites 4Ac-XN (**2**), 4Me-XN (**3**), XNC (**8**), and dhXNC (**9**). In relation to XN (**1**), the effect on cell viability and proliferation was slightly lower for 4Me-XN (**3**), which did not affect cell number

or cell cycle distribution up to a concentration of 50 µM. XNH (**5**) decreased cell viability but had a weaker impact on cell proliferation. Instead, it induced a G2/M arrest and a release of cytochrome c without altering the mitochondrial membrane potential. The differences might be due to higher hydrophilicity (log P value), lower cellular absorption, and altered cellular distribution.

In our assays, hydrogenation of the double bond in α,β position to the carbonyl group led to a loss of activity for dhFKC (**17**) and dhHeli (**18**), whereas thXNC (**19**) was still able to affect mitochondrial mass. This confirms that the Michael system constitutes a crucial structural element, however, substitution of the A ring as well drives chalcone activity and more importantly toxicity. P (**15**), with an unprotected hydroxyl group in position 6´, did not show any significant effects in our tests. The substitution pattern of the A ring clearly influenced activity of the investigated chalcones. By comparison, B ring substituents had a weaker impact, even favoring unsubstituted compounds such as C (**16**) and FKB (**13**). The 4´-methoxy derivatives FKB (**13**) and 4´Me-XN (**4**) were more cytotoxic than C (**16**) and XN (**1**).

No significant relationship between log P and activity of the chalcones was found (data not shown). In general, log P values between 1 and 4 are considered as beneficial for absorption. Relatively lipophilic chalcones like XN (**1**), generally show rapid cellular uptake, accumulation, and intracellular formation of protein complexes (thiol adducts) in hepatic stellate cells.

As the structural moieties are present in various combinations in the tested compounds, statistics can be performed on the observed phenotypes and presence of elements. We have performed analysis of covariance (ANCOVA) on the entire dataset to uncover correlations between substitutions to the basic chalcone scaffold and toxic effects on cells. **Figure 3** depicts all activities of individual elements, which reach a level of significance of at least $p \leq 0.05$.

Several conclusion could be drawn from these correlations: A pyrano-ring substitution at 3´/4´ position of the A-ring has a significant influence on proliferation, mitochondrial mass, nucleus area and cell cycle. The occurrence of a 3´-prenyl-chain significantly increases the

impact on proliferation, mitochondrial mass and cytochrome c release. An OH-group at position 4 of the B-ring correlates with an influence on actin, cell cycle, mitochondrial mass and cytochrome c release, whereas an OMe-group at the same position significantly influences the nucleus area. An OH- or OMe-group at position 3 of the B-ring is associated with an effect on cell proliferation, nucleus area, mitochondrial mass and actin.

The Michael-system constitutes a crucial structure element for an impact on proliferation, mitochondrial mass and cytochrome c release.

4. Discussion

In the past decade, chalcones were subject to a number of studies assessing their chemoprotective potential. However, it was not only found that chalcones have beneficial and protective activity, but it was also discovered that many of them have a strong cytotoxic potential and might cause severe adverse effects (Forejtníková et al., 2005; Orlikova et al., 2011). Several mechanisms have been identified, that are triggered by chalcone derivatives and mediate toxicity in mammalian cells. Some prominent ones being inhibition of tubulin assembly, cell cycle inhibition and mitotoxicity (Orlikova et al., 2011).

A number of studies have shown that anti-proliferative and cytotoxic effects correlate with the presence of hydroxyl substituents on the chalcone scaffold. Chalcones with hydroxyl groups seem to have more potent anti-proliferative properties than other chalcone derivatives, at least on cancer cells (Cabrera et al., 2007).

In the present study, we observed that XN (**1**) treatment leads to apoptosis, which has been described earlier to be mediated by activation of caspase 3 (Dorn et al., 2010). Other studies reported, that XN (**1**) treatment induced the mitochondrial-mediated pathways of programmed cell death in human colon carcinoma cells and caused a rapid breakdown of the mitochondrial membrane potential, and the release of cytochrome c, leading to apoptosis induction in BPH-1 cells (Strathmann et al., 2010). Our results propose that apoptosis caused by XN (**1**) is mediated by a loss of mitochondrial membrane potential and subsequent

cytochrome c release at concentrations as low as 10 µM, which is in good accordance with previous studies.

A prenyl group or a pyrano substitution seems to be a structural requirement for interaction with the mitochondrial membrane, as a decrease of mitochondrial mass was exclusively observed for these compounds. Further methoxy groups in the A ring increased particularly the anti-proliferative activity.

It is assumed that a prenylation of chalcones influences their solubility and lipophilicity (Gerhauser et al., 2002), thereby affecting cellular uptake and subcellular localization (Wolff et al., 2011). It can be speculated that this is crucial for cellular functions and toxic effects.

There is also evidence that 3,4,5-trimethoxy derivatization and an alpha-methyl group within the enone moiety influence microtubule depolymerization. Thus, alpha-methyl chalcones are believed to exhibit greater cytotoxic activity and inhibition of cell growth than unsubstituted analogues (Ducki, 2009; Ducki et al., 1998).

Our study once more confirmed that the Michael-system constitutes a crucial structural element for an impact on proliferation, mitochondrial mass and cytochrome c release. Hydrogenation of the double bond leads in most cases to a loss of activity. However, substitution of the A ring also drives chalcone activity and toxicity. An OH-group at position 6´ of the A-ring instead of a methoxy-group cannot be assigned to any specific activity, but reduced toxicity of the resulting chalcone.

Generally, previous findings are largely in good accordance with our data, but they did not reveal a clear relationship between toxicity and structural features. This may also be due to the fact, that various assays, different (cancer) cell types and data analysis methods have been employed by individual research groups. We have therefore chosen a set of easy to conduct assays and a single cell type to get data as consistent as possible.

Hepatic stellate cells are a highly suitable cell model, as a potential oral therapeutic or nutraceutical will inevitably have to pass the liver, where it might exhibit toxic (or beneficial) effects. We could show that the seven cellular features we used in our quantitative cell-based assays are able to reveal a broad range of phenotypic patterns caused by chalcones in

hepatic stellate cells. Although we cannot exclude, that we have missed toxic effects in our assays, only four compounds from 19 were determined to not have a significant toxic impact on the cells in the range from 10-50 µM. We have also observed 11 different patterns of up- and down-regulation of cellular features, which supports the conclusion, that our test-panel is sensitive and selective at the same time.

The results of the present study allow conclusions on two levels. On the one hand, we now have solid data on how individual chalcones affect activated hepatic stellate cells in respect to the measured features. On the other hand, we could draw conclusions about the effects for individual motifs and structural elements of chalcones.

We can imagine that this information can be useful to alter the activity or potency of other, slightly distinct chalcones. An exemplary candidate might be licochalcone A, which is known to inhibit cell cycle progression, to affect growth of cancer cells (Xiao et al., 2011) and to alter angiogenesis (Kim et al., 2010). Modifications proposed by our model could be used to either increase toxicity towards cancer cells, by e.g. introducing an OMe-group on position 3 of the B-ring, or to reduce toxicity while ideally keeping anti-angiogenic effects by removing the OH-group on position 4 of the B-ring.

As a final aspect, a thorough review of the activated hepatic stellate cell line as a test model for our assays, could also reveal some additional insights. *In vivo*, an activation of hepatic stellate cells can finally lead to the disease state of hepatic fibrosis. It was previously reported that F-actin cytoskeletal reorganization is an essential step in the activation of hepatic stellate cells (Cui et al., 2014). The cell model might therefore also be suitable to determine if and how substances alter the activation state and thereby a disease progression.

5. Conclusion

The results of the present study allow conclusions on how individual chalcone derivatives affect hepatic stellate cells, but even more how individual motifs and structural elements of

chalcones influence their cell toxicity. This information could be of great value for medicinal chemistry approaches and synthesis of chalcones with optimized structures and thus enhanced potency for distinct functions or targets. This includes for example the enhancement of pro-apoptotic or anti-proliferative effects of structures. On the other hand, undesirable cytotoxicity of chalcones with known and wanted effects on specific cellular parameters, e.g. transcription factors, could be reduced. Although it is open if other structurally related chalcones and motifs fall into the same scheme and will support our current observations, many reasonable permutations have already been addressed with the current approach. In future studies, the present data could additionally be compared with data generated with different cell types.

Acknowledgements

We thank Bionorica SE for supporting this work with the Bionorica Global Research Initiative Award. Jörg Heilmann (Institute of Pharmacy, University Regensburg) is gratefully acknowledged for scientific support and fruitful discussions.

Conflict of interest

The authors declare no conflicts of interest.

Figure and Table Legends

Figure 1: Overview over the chalcones investigated in this study. Structures on the left (A) possess a Michael-system, whereas structures on the right (B) do not have this element.

Figure 2: Overview of assay results for individual chalcone derivatives. Viability (MTT), proliferation (cell proliferation by cell number), nucleus area, actin filament area, mitochondrial mass, cytochrome c release, cell cycle. Individual compounds are grouped and up-and down-regulation of assay readouts are indicated.

Figure 3: Significant structure-toxicity relationships of distinct substitutions at the chalcone scaffold. The graphical representation depicts significant ($p < 0.05$) relationships between distinct substitutions and dose-dependent responses in cell-based assays.

Table 1: IC_{50} values of chalcones as determined by automatic cell counts and MTT assays. Dose response experiments for MTT assays were carried out up to 100 µM. Dose response experiments for cell counts were done up to 50 µM. If no statistically significant effect was observed up to 50 µM, *>>50 µM* is shown in the table. If there was a statistically significant decline ($p \leq 0.05$), but the response indicated an IC_{50} > 50 µM, *>50 µM* is shown. # = non-sigmoidal behavior of dose-response. n.d. = not done. For detailed information on cell count data see Supporting Information.

Table 2: Overview of assay results. Viability (MTT), proliferation (cell proliferation by cell number), nucleus area, actin filament area, mitochondrial mass, cytochrome c release, DNA content (cell cycle). (+) increase statistically significant at 50 µM, (++) increase statistically significant at 25 µM or less, (-) decrease statistically significant at 50 µM, (- -) decrease statistically significant at 25 µM or less, (0) not significant up to 50 µM. Distinct influence patterns were grouped with roman numbers from I to XI.

Supplementary Figure Legends

Supplementary Figure 1: Cell-based assay results for treatment of HSC with 1-50 µM xanthohumol (XN).

A) Cell number [%], value of untreated control cells (ctl) was set to 100%; **B)** nucleus area (area in pixels^2, value of untreated control cells (ctl) was set to 1); **C)** actin area (area in pixels^2, value of untreated control cells (ctl) was set to 1); **D)** cell cycle state (2N/4N ratio); **E)** mitochondrial fluorescence intensity [%], value of untreated control cells (ctl) was set as 100%; **F)** cytochrome c release [%], staurosporine-treatment (= positive control, p.ctl.) was set to 100%, value of untreated cells (= negative control, n.ctl.) was used as baseline. All values are presented as mean ± SD and refer to control cells (ctl, n.ctl.). Statistical analysis (one-way ANOVA following Dunnett's multi-comparison post-hoc test) was performed using GraphPad Prism 4 software. Levels of significance: *) $p \leq 0.05$, **) $p \leq 0.01$ vs ctl/n.ctl.

Supplementary Figure 2: Cell-based assay results for treatment of HSC with 1-50 µM 4-*O*-acetyl-xanthohumol (4Ac-XN).

A) Cell number [%], value of untreated control cells (ctl) was set to 100%; **B)** nucleus area (area in pixels^2, value of untreated control cells (ctl) was set to 1); **C)** actin area (area in pixels^2, value of untreated control cells (ctl) was set to 1); **D)** cell cycle state (2N/4N ratio); **E)** mitochondrial fluorescence intensity [%], value of untreated control cells (ctl) was set as 100%; **F)** cytochrome c release [%], staurosporine-treatment (= positive control, p.ctl.) was set to 100%, value of untreated cells (= negative control, n.ctl.) was used as baseline. All values are presented as mean ± SD and refer to control cells (ctl, n.ctl.). Statistical analysis (one-way ANOVA following Dunnett's multi-comparison post-hoc test) was performed using GraphPad Prism 4 software. Levels of significance: *) $p \leq 0.05$, **) $p \leq 0.01$ vs ctl/n.ctl.

Supplementary Figure 3: Cell-based assay results for treatment of HSC with 1-50 µM 4-*O*-methyl-xanthohumol (4Me-XN).

A) Cell number [%], value of untreated control cells (ctl) was set to 100%; **B)** nucleus area (area in pixels^2, value of untreated control cells (ctl) was set to 1); **C)** actin area (area in pixels^2, value of untreated control cells (ctl) was set to 1); **D)** cell cycle state (2N/4N ratio); **E)** mitochondrial fluorescence intensity [%], value of untreated control cells (ctl) was set as 100%; **F)** cytochrome c release [%], staurosporine-treatment (= positive control, p.ctl.) was set to 100%, value of untreated cells (= negative control, n.ctl.) was used as baseline. All values are presented as mean ± SD and refer to control cells (ctl, n.ctl.). Statistical analysis (one-way ANOVA following Dunnett's multi-comparison post-hoc test) was performed using GraphPad Prism 4 software. Levels of significance: *) $p \leq 0.05$, **) $p \leq 0.01$ vs ctl/n.ctl.

Supplementary Figure 4: Cell-based assay results for treatment of HSC with 1-50 µM 4'-*O*-methyl-xanthohumol (4'Me-XN).

A) Cell number [%], value of untreated control cells (ctl) was set to 100%; **B)** nucleus area (area in pixels^2, value of untreated control cells (ctl) was set to 1); **C)** actin area (area in pixels^2, value of untreated control cells (ctl) was set to 1); **D)** cell cycle state (2N/4N ratio); **E)** mitochondrial fluorescence intensity [%], value of untreated control cells (ctl) was set as 100%; **F)** cytochrome c release [%], staurosporine-treatment (= positive control, p.ctl.) was set to 100%, value of untreated cells (= negative control, n.ctl.) was used as baseline. All values are presented as mean ± SD and refer to control cells (ctl, n.ctl.). Statistical analysis (one-way ANOVA following Dunnett's multi-comparison post-hoc test) was performed using GraphPad Prism 4 software. Levels of significance: *) $p \leq 0.05$, **) $p \leq 0.01$ vs ctl/n.ctl.

Supplementary Figure 5: Cell-based assay results for treatment of HSC with 1-50 µM xanthohumol H (XNH).

A) Cell number [%], value of untreated control cells (ctl) was set to 100%; **B)** nucleus area (area in pixels^2, value of untreated control cells (ctl) was set to 1); **C)** actin area (area in pixels^2, value of untreated control cells (ctl) was set to 1); **D)** cell cycle state (2N/4N ratio); **E)** mitochondrial fluorescence intensity [%], value of untreated control cells (ctl) was set as 100%; **F)** cytochrome c release [%], staurosporine-treatment (= positive control, p.ctl.) was set to 100%, value of untreated cells (= negative control, n.ctl.) was used as baseline. All values are presented as mean ± SD and refer to control cells (ctl, n.ctl.). Statistical analysis (one-way ANOVA following Dunnett's multi-comparison post-hoc test) was performed using GraphPad Prism 4 software. Levels of significance: *) $p \leq 0.05$, **) $p \leq 0.01$ vs ctl/n.ctl.

Supplementary Figure 6: Cell-based assay results for treatment of HSC with 1-50 µM 3-hydroxy-xanthohumol H (3OH-XNH).

A) Cell number [%], value of untreated control cells (ctl) was set to 100%; **B)** nucleus area (area in pixels^2, value of untreated control cells (ctl) was set to 1); **C)** actin area (area in pixels^2, value of untreated control cells (ctl) was set to 1); **D)** cell cycle state (2N/4N ratio); **E)** mitochondrial fluorescence intensity [%], value of untreated control cells (ctl) was set as 100%; **F)** cytochrome c release [%], staurosporine-treatment (= positive control, p.ctl.) was set to 100%, value of untreated cells (= negative control, n.ctl.) was used as baseline. All values are presented as mean ± SD and refer to control cells (ctl, n.ctl.). Statistical analysis (one-way ANOVA following Dunnett's multi-comparison post-hoc test) was performed using GraphPad Prism 4 software. Levels of significance: *) $p \leq 0.05$, **) $p \leq 0.01$ vs ctl/n.ctl.

Supplementary Figure 7: Cell-based assay results for treatment of HSC with 1-50 µM 3-methoxy-xanthohumol H (3OMe-XNH).

A) Cell number [%], value of untreated control cells (ctl) was set to 100%; **B)** nucleus area (area in pixels^2, value of untreated control cells (ctl) was set to 1); **C)** actin area (area in pixels^2, value of untreated control cells (ctl) was set to 1); **D)** cell cycle state (2N/4N ratio); **E)** mitochondrial fluorescence intensity [%], value of untreated control cells (ctl) was set as 100%; **F)** cytochrome c release [%], staurosporine-treatment (= positive control, p.ctl.) was set to 100%, value of untreated cells (= negative control, n.ctl.) was used as baseline. All values are presented as mean ± SD and refer to control cells (ctl, n.ctl.). Statistical analysis (one-way ANOVA following Dunnett's multi-comparison post-hoc test) was performed using GraphPad Prism 4 software. Levels of significance: *) $p \leq 0.05$, **) $p \leq 0.01$ vs ctl/n.ctl.

Supplementary Figure 8: Cell-based assay results for treatment of HSC with 1-50 µM xanthohumol c (XNC).

A) Cell number [%], value of untreated control cells (ctl) was set to 100%; **B)** nucleus area (area in pixels^2, value of untreated control cells (ctl) was set to 1); **C)** actin area (area in pixels^2, value of untreated control cells (ctl) was set to 1); **D)** cell cycle state (2N/4N ratio); **E)** mitochondrial fluorescence intensity [%], value of untreated control cells (ctl) was set as 100%; **F)** cytochrome c release [%], staurosporine-treatment (= positive control, p.ctl.) was set to 100%, value of untreated cells (= negative control, n.ctl.) was used as baseline. All values are presented as mean ± SD and refer to control cells (ctl, n.ctl.). Statistical analysis (one-way ANOVA following Dunnett's multi-comparison post-hoc test) was performed using GraphPad Prism 4 software. Levels of significance: *) $p \leq 0.05$, **) $p \leq 0.01$ vs ctl/n.ctl.

Supplementary Figure 9: Cell-based assay results for treatment of HSC with 1-50 µM 1'',2''-dihydro-xanthohumol C (dhXNC).

A) Cell number [%], value of untreated control cells (ctl) was set to 100%; **B)** nucleus area (area in pixels^2, value of untreated control cells (ctl) was set to 1); **C)** actin area (area in pixels^2, value of untreated control cells (ctl) was set to 1); **D)** cell cycle state (2N/4N ratio); **E)** mitochondrial fluorescence intensity [%], value of untreated control cells (ctl) was set as 100%; **F)** cytochrome c release [%], staurosporine-treatment (= positive control, p.ctl.) was set to 100%, value of untreated cells (= negative control, n.ctl.) was used as baseline. All values are presented as mean ± SD and refer to control cells (ctl, n.ctl.). Statistical analysis (one-way ANOVA following Dunnett's multi-comparison post-hoc test) was performed using GraphPad Prism 4 software. Levels of significance: *) $p \leq 0.05$, **) $p \leq 0.01$ vs ctl/n.ctl.

Supplementary Figure 10: Cell-based assay results for treatment of HSC with 1-50 µM helichrysetin (Heli).

A) Cell number [%], value of untreated control cells (ctl) was set to 100%; **B)** nucleus area (area in pixels^2, value of untreated control cells (ctl) was set to 1); **C)** actin area (area in pixels^2, value of untreated control cells (ctl) was set to 1); **D)** cell cycle state (2N/4N ratio); **E)** mitochondrial fluorescence intensity [%], value of untreated control cells (ctl) was set as 100%; **F)** cytochrome c release [%], staurosporine-treatment (= positive control, p.ctl.) was set to 100%, value of untreated cells (= negative control, n.ctl.) was used as baseline. All values are presented as mean ± SD and refer to control cells (ctl, n.ctl.). Statistical analysis (one-way ANOVA following Dunnett's multi-comparison post-hoc test) was performed using GraphPad Prism 4 software. Levels of significance: *) $p \leq 0.05$, **) $p \leq 0.01$ vs ctl/n.ctl.

Supplementary Figure 11: Cell-based assay results for treatment of HSC with 1-50 µM 3-hydroxy-helichrysetin (3OH-Heli).

A) Cell number [%], value of untreated control cells (ctl) was set to 100%; **B)** nucleus area (area in pixels^2, value of untreated control cells (ctl) was set to 1); **C)** actin area (area in pixels^2, value of untreated control cells (ctl) was set to 1); **D)** cell cycle state (2N/4N ratio); **E)** mitochondrial fluorescence intensity [%], value of untreated control cells (ctl) was set as 100%; **F)** cytochrome c release [%], staurosporine-treatment (= positive control, p.ctl.) was set to 100%, value of untreated cells (= negative control, n.ctl.) was used as baseline. All values are presented as mean ± SD and refer to control cells (ctl, n.ctl.). Statistical analysis (one-way ANOVA following Dunnett's multi-comparison post-hoc test) was performed using GraphPad Prism 4 software. Levels of significance: *) $p \leq 0.05$, **) $p \leq 0.01$ vs ctl/n.ctl.

Supplementary Figure 12: Cell-based assay results for treatment of HSC with 1-50 µM flavokawain A (FKA).

A) Cell number [%], value of untreated control cells (ctl) was set to 100%; **B)** nucleus area (area in pixels^2, value of untreated control cells (ctl) was set to 1); **C)** actin area (area in pixels^2, value of untreated control cells (ctl) was set to 1); **D)** cell cycle state (2N/4N ratio); **E)** mitochondrial fluorescence intensity [%], value of untreated control cells (ctl) was set as 100%; **F)** cytochrome c release [%], staurosporine-treatment (= positive control, p.ctl.) was set to 100%, value of untreated cells (= negative control, n.ctl.) was used as baseline. All values are presented as mean ± SD and refer to control cells (ctl, n.ctl.). Statistical analysis (one-way ANOVA following Dunnett's multi-comparison post-hoc test) was performed using GraphPad Prism 4 software. Levels of significance: *) $p \leq 0.05$, **) $p \leq 0.01$ vs ctl/n.ctl.

Supplementary Figure 13: Cell-based assay results for treatment of HSC with 1-50 µM flavokawain B (FKB).

A) Cell number [%], value of untreated control cells (ctl) was set to 100%; **B)** nucleus area (area in pixels^2, value of untreated control cells (ctl) was set to 1); **C)** actin area (area in pixels^2, value of untreated control cells (ctl) was set to 1); **D)** cell cycle state (2N/4N ratio); **E)** mitochondrial fluorescence intensity [%], value of untreated control cells (ctl) was set as 100%; **F)** cytochrome c release [%], staurosporine-treatment (= positive control, p.ctl.) was set to 100%, value of untreated cells (= negative control, n.ctl.) was used as baseline. All values are presented as mean ± SD and refer to control cells (ctl, n.ctl.). Statistical analysis (one-way ANOVA following Dunnett's multi-comparison post-hoc test) was performed using GraphPad Prism 4 software. Levels of significance: *) $p \leq 0.05$, **) $p \leq 0.01$ vs ctl/n.ctl.

Supplementary Figure 14: Cell-based assay results for treatment of HSC with 1-50 µM flavokawain C (FKC).

A) Cell number [%], value of untreated control cells (ctl) was set to 100%; **B)** nucleus area (area in pixels^2, value of untreated control cells (ctl) was set to 1); **C)** actin area (area in pixels^2, value of untreated control cells (ctl) was set to 1); **D)** cell cycle state (2N/4N ratio); **E)** mitochondrial fluorescence intensity [%], value of untreated control cells (ctl) was set as 100%; **F)** cytochrome c release [%], staurosporine-treatment (= positive control, p.ctl.) was set to 100%, value of untreated cells (= negative control, n.ctl.) was used as baseline. All values are presented as mean ± SD and refer to control cells (ctl, n.ctl.). Statistical analysis (one-way ANOVA following Dunnett's multi-comparison post-hoc test) was performed using GraphPad Prism 4 software. Levels of significance: *) $p \leq 0.05$, **) $p \leq 0.01$ vs ctl/n.ctl.

Supplementary Figure 15: Cell-based assay results for treatment of HSC with 1-50 µM pinostrobin chalcone (P).

A) Cell number [%], value of untreated control cells (ctl) was set to 100%; **B)** nucleus area (area in pixels^2, value of untreated control cells (ctl) was set to 1); **C)** actin area (area in pixels^2, value of untreated control cells (ctl) was set to 1); **D)** cell cycle state (2N/4N ratio); **E)** mitochondrial fluorescence intensity [%], value of untreated control cells (ctl) was set as 100%; **F)** cytochrome c release [%], staurosporine-treatment (= positive control, p.ctl.) was set to 100%, value of untreated cells (= negative control, n.ctl.) was used as baseline. All values are presented as mean ± SD and refer to control cells (ctl, n.ctl.). Statistical analysis (one-way ANOVA following Dunnett's multi-comparison post-hoc test) was performed using GraphPad Prism 4 software. Levels of significance: *) $p \leq 0.05$, **) $p \leq 0.01$ vs ctl/n.ctl.

Supplementary Figure 16: Cell-based assay results for treatment of HSC with 1-50 µM cardamonin (C).

A) Cell number [%], value of untreated control cells (ctl) was set to 100%; **B)** nucleus area (area in pixels^2, value of untreated control cells (ctl) was set to 1); **C)** actin area (area in pixels^2, value of untreated control cells (ctl) was set to 1); **D)** cell cycle state (2N/4N ratio); **E)** mitochondrial fluorescence intensity [%], value of untreated control cells (ctl) was set as 100%; **F)** cytochrome c release [%], staurosporine-treatment (= positive control, p.ctl.) was set to 100%, value of untreated cells (= negative control, n.ctl.) was used as baseline. All values are presented as mean ± SD and refer to control cells (ctl, n.ctl.). Statistical analysis (one-way ANOVA following Dunnett's multi-comparison post-hoc test) was performed using GraphPad Prism 4 software. Levels of significance: *) $p \leq 0.05$, **) $p \leq 0.01$ vs ctl/n.ctl.

Supplementary Figure 17: Cell-based assay results for treatment of HSC with 1-50 µM dihydro-flavokawain C (dhFKC).

A) Cell number [%], value of untreated control cells (ctl) was set to 100%; **B)** nucleus area (area in pixels^2, value of untreated control cells (ctl) was set to 1); **C)** actin area (area in pixels^2, value of untreated control cells (ctl) was set to 1); **D)** cell cycle state (2N/4N ratio); **E)** mitochondrial fluorescence intensity [%], value of untreated control cells (ctl) was set as 100%; **F)** cytochrome c release [%], staurosporine-treatment (= positive control, p.ctl.) was set to 100%, value of untreated cells (= negative control, n.ctl.) was used as baseline. All values are presented as mean ± SD and refer to control cells (ctl, n.ctl.). Statistical analysis (one-way ANOVA following Dunnett's multi-comparison post-hoc test) was performed using GraphPad Prism 4 software. Levels of significance: *) $p \leq 0.05$, **) $p \leq 0.01$ vs ctl/n.ctl.

Supplementary Figure 18: Cell-based assay results for treatment of HSC with 1-50 µM dihydro-helichrysetin (dhHeli).

A) Cell number [%], value of untreated control cells (ctl) was set to 100%; **B)** nucleus area (area in pixels^2, value of untreated control cells (ctl) was set to 1); **C)** actin area (area in pixels^2, value of untreated control cells (ctl) was set to 1); **D)** cell cycle state (2N/4N ratio); **E)** mitochondrial fluorescence intensity [%], value of untreated control cells (ctl) was set as 100%; **F)** cytochrome c release [%], staurosporine-treatment (= positive control, p.ctl.) was set to 100%, value of untreated cells (= negative control, n.ctl.) was used as baseline. All values are presented as mean ± SD and refer to control cells (ctl, n.ctl.). Statistical analysis (one-way ANOVA following Dunnett's multi-comparison post-hoc test) was performed using GraphPad Prism 4 software. Levels of significance: *) $p \leq 0.05$, **) $p \leq 0.01$ vs ctl/n.ctl.

Supplementary Figure 19: Cell-based assay results for treatment of HSC with 1-50 µM dihydro-1'',2''-dihydro-xanthohumol C (thXNC).

A) Cell number [%], value of untreated control cells (ctl) was set to 100%; **B)** nucleus area (area in pixels^2, value of untreated control cells (ctl) was set to 1); **C)** actin area (area in pixels^2, value of untreated control cells (ctl) was set to 1); **D)** cell cycle state (2N/4N ratio); **E)** mitochondrial fluorescence intensity [%], value of untreated control cells (ctl) was set as 100%; **F)** cytochrome c release [%], staurosporine-treatment (= positive control, p.ctl.) was set to 100%, value of untreated cells (= negative control, n.ctl.) was used as baseline. All values are presented as mean ± SD and refer to control cells (ctl, n.ctl.). Statistical analysis (one-way ANOVA following Dunnett's multi-comparison post-hoc test) was performed using GraphPad Prism 4 software. Levels of significance: *) $p \leq 0.05$, **) $p \leq 0.01$ vs ctl/n.ctl.

References

Batovska, D.I., Todorova, I.T., 2010. Trends in utilization of the pharmacological potential of chalcones. Curr Clin Pharmacol 5, 1–29.

Bickle, M., 2010. The beautiful cell: high-content screening in drug discovery. Anal Bioanal Chem 398, 219–26. doi:10.1007/s00216-010-3788-3

Cabrera, M., Simoens, M., Falchi, G., Lavaggi, M.L., Piro, O.E., Castellano, E.E., Vidal, A., Azqueta, A., Monge, A., de Ceráin, A.L., Sagrera, G., Seoane, G., Cerecetto, H., González, M., 2007. Synthetic chalcones, flavanones, and flavones as antitumoral agents: biological evaluation and structure-activity relationships. Bioorg. Med. Chem. 15, 3356–67.

Chadwick, L.R., Nikolic, D., Burdette, J.E., Overk, C.R., Bolton, J.L., van Breemen, R.B., Fröhlich, R., Fong, H.H.S., Farnsworth, N.R., Pauli, G.F., 2004. Estrogens and congeners from spent hops (Humulus lupulus). J. Nat. Prod. 67, 2024–32. doi:10.1021/np049783i

Cui, X., Zhang, X., Yin, Q., Meng, A., Su, S., Jing, X., Li, H., Guan, X., Li, X., Liu, S., Cheng, M., 2014. F‐actin cytoskeleton reorganization is associated with hepatic stellate cell activation. Mol Med Rep 9, 1641–7. doi:10.3892/mmr.2014.2036

Das, S., Mitra, I., Batuta, S., Niharul Alam, M., Roy, K., Begum, N.A., 2014. Design, synthesis and exploring the quantitative structure-activity relationship of some antioxidant flavonoid analogues. Bioorg. Med. Chem. Lett. 24, 5050–4. doi:10.1016/j.bmcl.2014.09.028

Dimmock, J.R., Elias, D.W., Beazely, M.A., Kandepu, N.M., 1999. Bioactivities of chalcones. Curr. Med. Chem. 6, 1125–49.

Dorn, C., Kraus, B., Motyl, M., Weiss, T.S., Gehrig, M., Schölmerich, J., Heilmann, J., Hellerbrand, C., 2010. Xanthohumol, a chalcon derived from hops, inhibits hepatic inflammation and fibrosis. Mol Nutr Food Res 54 Suppl 2, S205–13. doi:10.1002/mnfr.200900314

Ducki, S., 2009. Antimitotic chalcones and related compounds as inhibitors of tubulin assembly. Anticancer Agents Med Chem 9, 336–47.

Ducki, S., Forrest, R., Hadfield, J.A., Kendall, A., Lawrence, N.J., McGown, A.T., Rennison, D., 1998. Potent antimitotic and cell growth inhibitory properties of substituted chalcones. Bioorg. Med. Chem. Lett. 8, 1051–6.

Field, C.M., Lénárt, P., 2011. Bulk cytoplasmic actin and its functions in meiosis and mitosis. Curr. Biol. 21, R825–30. doi:10.1016/j.cub.2011.07.043

Forejtníková, H., Lunerová, K., Kubínová, R., Jankovská, D., Marek, R., Kares, R., Suchý, V., Vondrácek, J., Machala, M., 2005. Chemoprotective and toxic potentials of synthetic and natural chalcones and dihydrochalcones in vitro. Toxicology 208, 81–93.

Freischmidt, A., Jürgenliemk, G., Kraus, B., Okpanyi, S.N., Müller, J., Kelber, O., Weiser, D., Heilmann, J., 2012. Contribution of flavonoids and catechol to the reduction of ICAM-1 expression in endothelial cells by a standardised Willow bark extract. Phytomedicine 19, 245–52. doi:10.1016/j.phymed.2011.08.065

Furusawa, J., Funakoshi-Tago, M., Mashino, T., Tago, K., Inoue, H., Sonoda, Y., Kasahara, T., 2009. Glycyrrhiza inflata-derived chalcones, Licochalcone A, Licochalcone B and Licochalcone D, inhibit phosphorylation of NF-kappaB p65 in LPS signaling pathway. Int. Immunopharmacol. 9, 499–507.

Gasparri, F., Cappella, P., Galvani, A., 2006. Multiparametric cell cycle analysis by automated microscopy. J Biomol Screen 11, 586–98.

Gaucher, M., Dugé de Bernonville, T., Lohou, D., Guyot, S., Guillemette, T., Brisset, M.-N., Dat, J.F., 2013. Histolocalization and physico-chemical characterization of dihydrochalcones: Insight into the role of apple major flavonoids. Phytochemistry 90, 78–89. doi:10.1016/j.phytochem.2013.02.009

Gerhauser, C., Alt, A., Heiss, E., Gamal-Eldeen, A., Klimo, K., Knauft, J., Neumann, I., Scherf, H.-R., Frank, N., Bartsch, H., Becker, H., 2002. Cancer chemopreventive activity of Xanthohumol, a natural product derived from hop. Mol. Cancer Ther. 1, 959–69.

Hanske, L., Loh, G., Sczesny, S., Blaut, M., Braune, A., 2010. Recovery and metabolism of xanthohumol in germ-free and human microbiota-associated rats. Mol Nutr Food Res 54, 1405–13. doi:10.1002/mnfr.200900517

Harikumar, K.B., Kunnumakkara, A.B., Ahn, K.S., Anand, P., Krishnan, S., Guha, S., Aggarwal, B.B., 2009. Modification of the cysteine residues in IkappaBalpha kinase and NF-kappaB (p65) by xanthohumol leads to suppression of NF-kappaB-regulated gene products and potentiation of apoptosis in leukemia cells. Blood 113, 2003–13. doi:10.1182/blood-2008-04-151944

He, X.G., Lin, L.Z., Lian, L.Z., 1997. Electrospray high performance liquid chromatography-mass spectrometry in phytochemical analysis of kava (Piper methysticum) extract. Planta Med. 63, 70–4.

Hellerbrand, C., 2013. Hepatic stellate cells-the pericytes in the liver. Pflugers Arch. 465, 775–8. doi:10.1007/s00424-012-1209-5

Henderson, M.C., Miranda, C.L., Stevens, J.F., Deinzer, M.L., Buhler, D.R., 2000. In vitro inhibition of human P450 enzymes by prenylated flavonoids from hops, Humulus lupulus. Xenobiotica 30, 235–51. doi:10.1080/004982500237631

Iwase, Y., Takahashi, M., Takemura, Y., Ju-ichi, M., Ito, C., Furukawa, H., Yano, M., 2001. Isolation and identification of two new flavanones and a chalcone from Citrus kinokuni. Chem. Pharm. Bull. 49, 1356–8.

Jung, H., Shin, S.Y., Jung, Y., Tran, T.A., Lee, H.O., Jung, K.-Y., Koh, D., Cho, S.K., Lim, Y., 2015. Quantitative relationships between the cytotoxicity of flavonoids on the human breast cancer stem-like cells MCF7-SC and their structural properties. Chem Biol Drug

Des. doi:10.1111/cbdd.12512

Kim, H.J., Lee, I.-S., 2006. Microbial metabolism of the prenylated chalcone xanthohumol. J. Nat. Prod. 69, 1522–4. doi:10.1021/np060310g

Kim, H.J., Shin, E.K., Kim, D.H., Lee, H.H., Park, J.H.Y., Kim, J.-K., 2010. Antiangiogenic effect of licochalcone A. Biochem. Pharm. 80, 1152-9.

Legette, L., Karnpracha, C., Reed, R.L., Choi, J., Bobe, G., Christensen, J.M., Rodriguez-Proteau, R., Purnell, J.Q., Stevens, J.F., 2014. Human pharmacokinetics of xanthohumol, an antihyperglycemic flavonoid from hops. Mol Nutr Food Res 58, 248–55. doi:10.1002/mnfr.201300333

Liu, M., Hansen, P.E., Wang, G., Qiu, L., Dong, J., Yin, H., Qian, Z., Yang, M., Miao, J., 2015. Pharmacological Profile of Xanthohumol, a Prenylated Flavonoid from Hops (Humulus lupulus). Molecules 20, 754–779. doi:10.3390/molecules20010754

Magalhães, P.J., Carvalho, D.O., Cruz, J.M., Guido, L.F., Barros, A.A., 2009. Fundamentals and health benefits of xanthohumol, a natural product derived from hops and beer. Nat Prod Commun 4, 591–610.

Malek, S.N.A., Phang, C.W., Ibrahim, H., Norhanom, A.W., Sim, K.S., 2011. Phytochemical and cytotoxic investigations of Alpinia mutica rhizomes. Molecules 16, 583–9. doi:10.3390/molecules16010583

Mohamad, H., Abas, F., Permana, D., Lajis, N.H., Ali, A.M., Sukari, M.A., Hin, T.Y.Y., Kikuzaki, H., Nakatani, N., 2004. DPPH free radical scavenger components from the fruits of Alpinia rafflesiana Wall. ex. Bak. (Zingiberaceae). Z. Naturforsch., C, J. Biosci. 59, 811–5.

Mosmann, T., 1983. Rapid colorimetric assay for cellular growth and survival: application to proliferation and cytotoxicity assays. J. Immunol. Methods 65, 55–63.

Nikolic, D., Li, Y., Chadwick, L.R., Pauli, G.F., van Breemen, R.B., 2005. Metabolism of xanthohumol and isoxanthohumol, prenylated flavonoids from hops (Humulus lupulus L.), by human liver microsomes. J Mass Spectrom 40, 289–99. doi:10.1002/jms.753

Nookandeh, A., Frank, N., Steiner, F., Ellinger, R., Schneider, B., Gerhäuser, C., Becker, H., 2004. Xanthohumol metabolites in faeces of rats. Phytochemistry 65, 561–70. doi:10.1016/j.phytochem.2003.11.016

Orlikova, B., Tasdemir, D., Golais, F., Dicato, M., Diederich, M., 2011. Dietary chalcones with chemopreventive and chemotherapeutic potential. Genes Nutr 6, 125–47. doi:10.1007/s12263-011-0210-5

Pang, Y., Nikolic, D., Zhu, D., Chadwick, L.R., Pauli, G.F., Farnsworth, N.R., van Breemen, R.B., 2007. Binding of the hop (Humulus lupulus L.) chalcone xanthohumol to cytosolic proteins in Caco-2 intestinal epithelial cells. Mol Nutr Food Res 51, 872–9. doi:10.1002/mnfr.200600252

Sahu, N.K., Balbhadra, S.S., Choudhary, J., Kohli, D.V., 2012. Exploring pharmacological significance of chalcone scaffold: a review. Curr. Med. Chem. 19, 209–25.

Scatena, R., 2012. Mitochondria and drugs. Adv. Exp. Med. Biol. 942, 329–46. doi:10.1007/978-94-007-2869-1_15

Schnabl, B., Choi, Y.H., Olsen, J.C., Hagedorn, C.H., Brenner, D.A., 2002. Immortal activated human hepatic stellate cells generated by ectopic telomerase expression. Lab. Invest. 82, 323–33.

Stevens, J.F., Taylor, A.W., Nickerson, G.B., Ivancic, M., Henning, J., Haunold, A., Deinzer, M.L., 2000. Prenylflavonoid variation in Humulus lupulus: distribution and taxonomic significance of xanthogalenol and 4'-O-methylxanthohumol. Phytochemistry 53, 759–75.

Strathmann, J., Klimo, K., Sauer, S.W., Okun, J.G., Prehn, J.H.M., Gerhäuser, C., 2010. Xanthohumol-induced transient superoxide anion radical formation triggers cancer cells into apoptosis via a mitochondria-mediated mechanism. FASEB J. 24, 2938–50. doi:10.1096/fj.10-155846

Van Puyvelde, L., De Kimpe, N., Costa, J., Munyjabo, V., Nyirankuliza, S., Hakizamungu, E., Schamp, N., 1989. Isolation of flavonoids and a chalcone from Helichrysum odoratissimum and synthesis of helichrysetin. J. Nat. Prod. 52, 629–33.

Vogel, S., Barbic, M., Jürgenliemk, G., Heilmann, J., 2010. Synthesis, cytotoxicity, anti-oxidative and anti-inflammatory activity of chalcones and influence of A-ring modifications on the pharmacological effect. Eur J Med Chem 45, 2206–13. doi:10.1016/j.ejmech.2010.01.060

Vogel, S., Heilmann, J., 2008. Synthesis, cytotoxicity, and antioxidative activity of minor prenylated chalcones from Humulus lupulus. J. Nat. Prod. 71, 1237–41. doi:10.1021/np800188b

Vogel, S., Ohmayer, S., Brunner, G., Heilmann, J., 2008. Natural and non-natural prenylated chalcones: synthesis, cytotoxicity and anti-oxidative activity. Bioorg. Med. Chem. 16, 4286–93. doi:10.1016/j.bmc.2008.02.079

Wolff, H., Motyl, M., Hellerbrand, C., Heilmann, J., Kraus, B., 2011. Xanthohumol uptake and intracellular kinetics in hepatocytes, hepatic stellate cells, and intestinal cells. J. Agric. Food Chem. 59, 12893–901. doi:10.1021/jf203689z

Xiao, X.-Y., Hao, M., Yang, X.-Y., Ba, Q., Li, M., Ni, S.-J. Wang, L.-S., Du, X., 2011. Licochalcone A inhibits growth of gastric cancer cells by arresting cell cycle progression and inducing apoptosis. Can. Let. 302, 69-75.

Xie, Y., Yang, W., Tang, F., Chen, X., Ren, L., 2015. Antibacterial activities of flavonoids: structure-activity relationship and mechanism. Curr. Med. Chem. 22, 132–49.

Xiong, S., Mu, T., Wang, G., Jiang, X., 2014. Mitochondria-mediated apoptosis in mammals. Protein Cell 5, 737–49. doi:10.1007/s13238-014-0089-1

Yamamoto, T., Yoshimura, M., Yamaguchi, F., Kouchi, T., Tsuji, R., Saito, M., Obata, A., Kikuchi, M., 2004. Anti-allergic activity of naringenin chalcone from a tomato skin extract. Biosci. Biotechnol. Biochem. 68, 1706–11. doi:10.1271/bbb.68.1706

Yilmazer, M., Stevens, J.F., Buhler, D.R., 2001a. In vitro glucuronidation of xanthohumol, a flavonoid in hop and beer, by rat and human liver microsomes. FEBS Lett. 491, 252–6.

Yilmazer, M., Stevens, J.F., Deinzer, M.L., Buhler, D.R., 2001b. In vitro biotransformation of xanthohumol, a flavonoid from hops (Humulus lupulus), by rat liver microsomes. Drug Metab. Dispos. 29, 223–31.

Zock, J.M., 2009. Applications of high content screening in life science research. Comb. Chem. High Throughput Screen. 12, 870–76.

Table 1

		IC_{50} in µM	
No	**Short Name**	**MTT**	**Cell Count**
1	XN	65 ± 4	>50
2	4Ac-XAN	75 ± 7	>50
3	4Me-XAN	#	>>50
4	4'Me-XAN	n.d.	30 ± 5
5	XNH	49 ± 6	>50
6	3OH-XNH	n.d.	>50
7	3OMe-XNH	>100	>50
8	XNC	69 ± 3	>50
9	dhXNC	55 ± 4	>50
10	Heli	97 ± 2	>50
11	3OH-Heli	>100	>>50
12	FKA	90 ± 12	>50
13	FKB	39 ± 3	43 ± 10
14	FKC	76 ± 8	>50

15	P	#	>>50
16	C	>100	>50
17	dhFKC	>100	>>50
18	dhHeli	>100	>>50
19	thXANC	>100	>>50

Table 2

No.	Short Name	Viability	Proliferation	Nucleus Area	Actin-Filament Area	Mitochondrial mass	Cytochrome c	Cell Cycle	GROUPING
1	XN	-	-	+	0	- -	+ +	+	**I**
2	4Ac-XN	-	-	+	0	- -	+ +	+	**I**
3	4Me-XN	-	0	-	0	- -	+	0	**II**
4	4'Me-XN	-	- -	-	-	- -	+	+	**III**
5	XNH	- -	0	+	0	0	+ +	+	**IV**
6	3OH-XNH	-	- -	+	0	-	+ +	+	**V**
7	3OMe-XNH	-	-	+	0	0	+	+	**V**
8	XNC	-	-	+	0	- -	+ +	+	**I**
9	dhXNC	-	-	+	0	- -	+ +	+	**I**
10	Heli	-	-	+	0	0	+ +	0	**VI**
11	3OH-Heli	0	0	0	0	0	0	0	**VII**
12	FKA	-	-	+ +	+	+	+ +	+	**VIII**
13	FKB	-	-	0	+	+ +	+ +	0	**IX**
14	FKC	-	-	+	0	0	0	+	**X**
15	P	0	0	0	0	0	0	0	**VII**
16	C	-	- -	+	+ +	+	+ +	+ +	**VIII**
17	dhFKC	0	0	0	0	0	0	0	**VII**
18	dhHeli	0	0	0	0	0	0	0	**VII**
19	thXNC	0	0	0	0	- -	+	0	**XI**

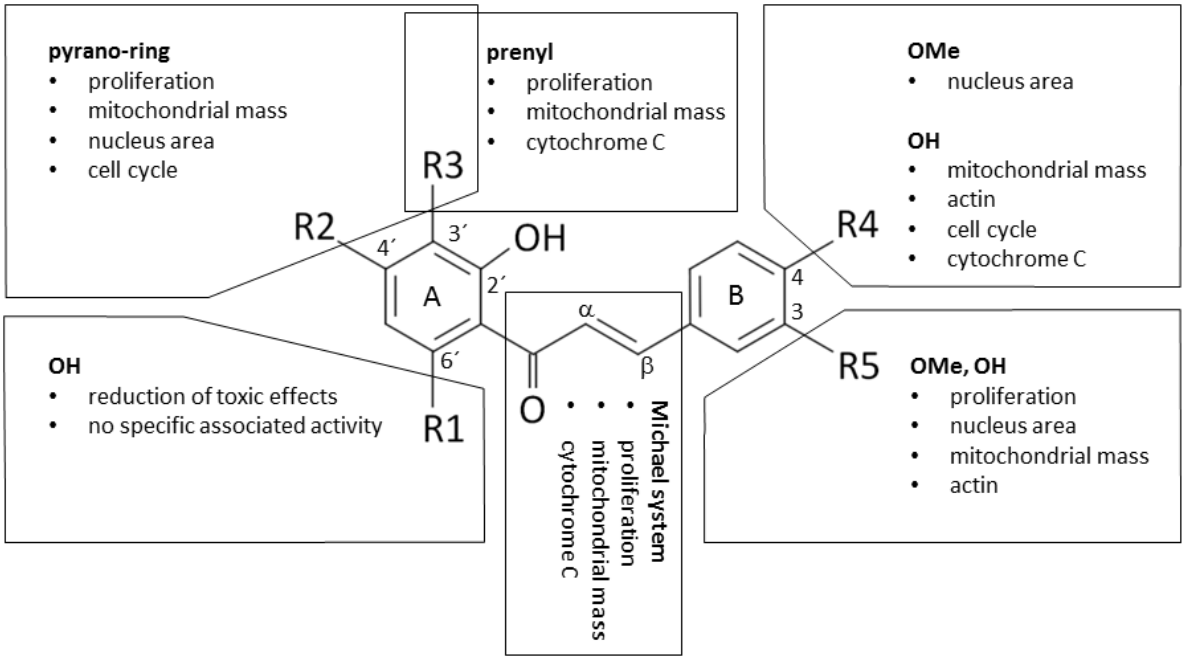

Figure3n .

A)

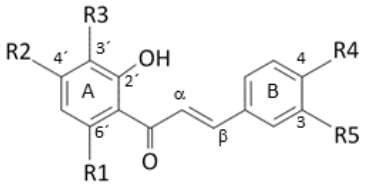

No	Short	R1	R2	R3	R4	R5
1	XN	OMe	OH		OH	H
2	4Ac-XN	OMe	OH		OAc	H
3	4Me-XN	OMe	OH		OMe	H
4	4'Me-XN	OMe	OMe		OH	H
5	XNH	OMe	OH		OH	H
6	3OH-XNH	OMe	OH		OH	OH
7	3OMe-XNH	OMe	OH		OH	OMe
8	XNC	OMe			OH	H
9	dhXNC	OMe			OH	H
10	Heli	OMe	OH	H	OH	H
11	3OH-Heli	OMe	OH	H	OH	OH
12	FKA	OMe	OMe	H	OMe	H
13	FKB	OMe	OMe	H	H	H
14	FKC	OMe	OMe	H	OH	H
15	P	OH	OMe	H	H	H
16	C	OMe	OH	H	H	H

B)

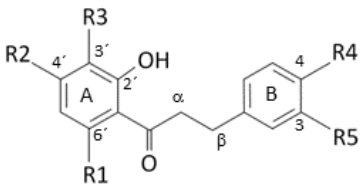

No	Short	R1	R2	R3	R4	R5
17	dhFKC	OMe	OMe	H	OH	H
18	dhHeli	OMe	OH	H	OH	H
19	thXNC	OMe			OH	H

Figure_1 .

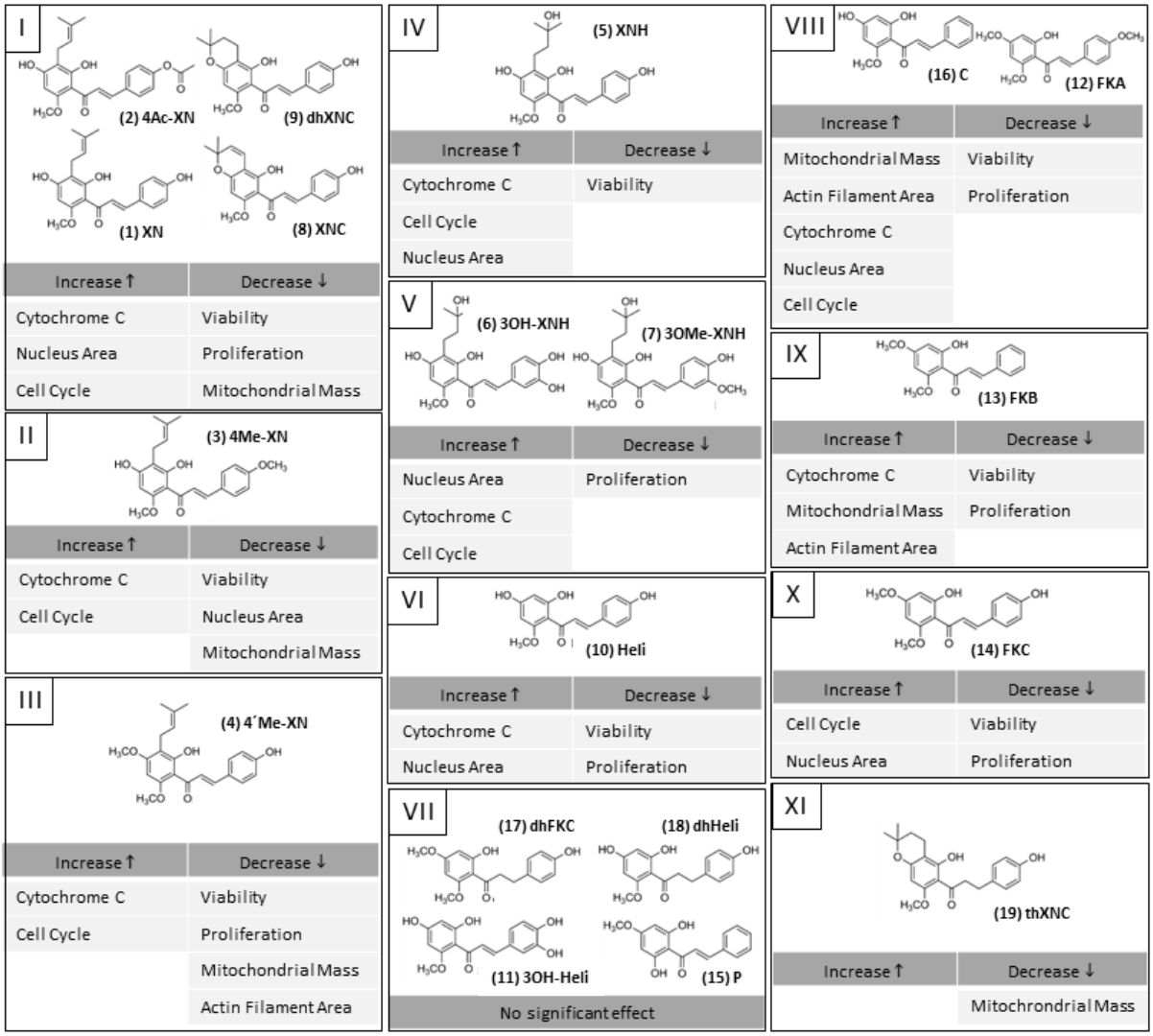

Figure_2 .